Available online at www.sciencedirect.com
ScienceDirect
Ceramics International 36 (2010) 1805–1816
CERAMICS INTERNATIONAL
www.elsevier.com/locate/ceramint

# The effect of surface treatment on CaP deposition of Ti6Al4V open cell foams in SBF solution

Ugur Turkan [a,1], Mustafa Guden [a,b,c,*]

[a] Department of Mechanical Engineering, Izmir Institute of Technology, Gulbahce Köyu, Urla, 35430 Izmir, Turkey
[b] Center for Materials Research, Izmir Institute of Technology, Gulbahce Koyu, Urla, 35430 Izmir, Turkey
[c] Dynamic Testing and Modeling Laboratory, Izmir Institute of Technology, Gulbahce Koyu, Urla, 35430 Izmir, Turkey

Received 2 November 2009; received in revised form 3 February 2010; accepted 10 March 2010
Available online 28 April 2010

**Abstract**

The effects of alkali and nitric acid surface treatment and acid etching on the CaP deposition of an open cell Ti6Al4V foam (60% porous and 300–500 μm in pore size) developed for biomedical applications were investigated in a simulated body fluid (SBF) solution for 14-day. The surface roughness of the foam specimens ground flat surfaces was measured in nano-metric scale before and after SBF immersion using an atomic force microscope (AFM). A significant increase in the surface roughness of alkali treated foam specimen after SBF immersion indicated a smaller crystal size CaP deposition, which was also confirmed by the AFM micrographs. The microscopic evaluation clearly showed that alkali treatment and nitric acid treatment induced a continuous, uniform CaP deposition on the cell wall surfaces of the foam (interior of cells). While in untreated foam specimen the cells are filled with CaP precipitates and acid etching did not produce a continuous coating layer on particles interior of the cells. The coating layer thickness was ~3 μm in alkali treated foam specimens after 14-day of SBF immersion, while nitric acid treatment induced relatively thinner coating layer, 0.6 μm.


*Keywords:* A. Films; B. Surfaces; D. Apatite; E. Biomedical applications

## 1. Introduction

Porous Ti and Ti6Al4V (Ti64) alloy implants are known to provide better interaction with bone due to the higher degree of bone in-growth and body fluid transport through three-dimensional interconnected arrays of pores, leading to improved implant fixation [1]. The implants of porous materials also reduce the extent of well-known stress shielding, which causes the implant loosening [2]. The current methods of porous Ti and Ti64 alloy processing are virtually based on powder sintering methods, namely the sintering green powder compacts and the space holder method [3]. In the sintering powder compacts method, relatively large powder sizes are generally used; however, the method inherently produces relatively small pore size and low porosity. The pore size and porosity typically range between 53 and 85 μm and 5 and 54%, respectively [4–6]. In contrast, the space holder method comes up with relatively larger pore sizes, 200–500 μm, and higher porosities, up to 80% [7]. Both methods; however, allow the direct near net-shape fabrications of porous implant components having elastic modulus and strength values comparable with those of natural bone [4,6]. Certain implant applications of Ti alloy foams have also been recently exploited including spinal cages used in spinal surgery for bone fixation [8]. Since these applications require relatively shorter bone fixation periods onto the porous surface, calcium phosphate (CaP) coating of porous surfaces including Ti mesh [9,10] and the sintered beads surface coatings [11,12] were previously investigated. Various surface treatments were further applied in conjunction with biomimetic CaP coating to fulfill the requirement for in vivo bone growth namely the formation of CaP (bone like apatite). Bone like apatite coating on Ti improves the surface osteoblast cell adhesion and differentiation [13] and increases the bone bonding strength by allowing an early bone opposition to the implant [14].

* Corresponding author at: Department of Mechanical Engineering, Izmir Institute of Technology, Gulbahce Köyu, Urla, 35430 Izmir, Turkey.
Tel.: +90 232 7506779; fax: +90 232 7506701.
*E-mail addresses:* ugurturkan@iyte.edu.tr (U. Turkan), mustafaguden@iyte.edu.tr (M. Guden).
[1] Tel.: +90 232 7506789; fax: +90 232 7506701.

0272-8842/$36.00 
doi:10.1016/j.ceramint.2010.03.030

Zhang et al. [15] investigated the biomimetic and electrochemical CaP deposition on a 40% porous and 100–300 μm pore size sintered Ti powder compact. The compact specimens were acid etched (AE) and then alkali treated (AT) without subsequent heat treatment before immersing into simulated body fluid (SBF). The results showed that after 6-day of SBF immersion, a continuous, homogeneous CaP coating layer formed in AT compact specimens, whereas no CaP coating layer formation was observed in AE specimens. It was emphasized that alkali treatment was a prerequisite for a uniform CaP coating layer deposition on the inner pores of the compacts; while, the electrochemical deposition resulted in less uniform coating layer, which was mainly attributed to the non-uniform current distribution in the porous structure. Liang et al. [16] studied the effect of alkali treatment and subsequent heat-treatment process on CaP deposition in a 40% porous and 250 μm pore size sintered Ti powder compact. The size of porous network structure (sodium titanate hydrogel) was shown to increase with increasing molar concentration of NaOH. In compact specimens with smaller pores of network structure, no apatite coating layer was detected after 28-day of SBF immersion. The lack of apatite formation on the compact particle surfaces with smaller pore sizes of network structure was attributed to low solute concentrations reaching inside the pores. Furthermore, the cell attachment and proliferation increased in an Ti64 alloy, when the surface roughness increased from 0.25 to 0.87 μm [17]. A critical molar concentration of NaOH (10 M), after which a smooth surface layer formed and resulted in no apatite nucleation after 3-day of SBF immersion was also reported [18]. The effect of subsequent heat treatment was found to increase the adherence of sodium titanate layer to Ti substrate [18] and induce a finer porous reticulate structure [19].

The previous investigations outlined above were mainly concentrated on CaP deposition in sintered powder compacts in which the pore size and porosity levels were comparably low. The present study was therefore conducted in order to investigate the effect of widely applied surface treatments of Ti and its alloys including alkali and nitric acid surface treatment and acid etching on biomimetic CaP deposition in an open cell Ti64 foam, potentially being used in hard tissue applications. Furthermore, the surface roughness of the foam flat surfaces, before and after deposition, was measured in nano-meter scale to assess the effect of surface roughness on CaP deposition. The major requirements of CaP deposition of foamy biomedical structures may include (a) forming a uniform coating layer on the cell edges and interior surfaces of the cells or pores and (b) maintaining the open cell structure of the foam after coating.

## 2. Materials and methods

### 2.1. Foam preparation and surface treatments

Interconnected open cell Ti64 alloy foams were prepared using the space holder method [7]. In this method, the metal powder is mixed with a suitable space holding material which decomposes at relatively low temperatures. Then, the powder mixture is compacted under uniaxial pressure to form a green compact. At an intermediate stage, the space holder material is removed and the resultant open cell green compact is sintered at a relatively high temperature. Gas atomized spherical Ti64 alloy powder (Crucible Research), of which the chemical composition was complied with ASTM 1580-1 standard [20] was used to prepare foam specimens (Table 1). The particle size of Ti64 powder ranged between 45 and 150 μm and nearly 80% of the particles were larger than 63 μm, showing a near mono modal particle size distribution (Table 2). Ammonium bicarbonate (Aldrich) powder with a particle size range of 315–500 μm was used as space holding material with an addition of 60 vol%. The green powder compacts, 40 mm × 40 mm × 10 mm in size, were compacted at room temperature inside a tool steel die at a uniaxial pressure of 200 MPa using a polyvinyl alcohol solution (10% by volume) as binder in an amount of 2% by weight. The space holder was removed at 200 °C with a heating duration of 2 h. In the final stage, the green compacts were sintered at 1300 °C for 2 h under a high purity (99.998%) Ar flux (400 $cm^3$/min). During heating cycle under Ar flux, the compacts were kept at 500 °C for 0.5 h in order to allow the complete burning-off of the binder. The compacts were heated and cooled at a rate of 5 °C $min^{-1}$. The foams prepared with the abovementioned method contained nearly 60% porosity with a bimodal pore size distribution: macropores (300–500 μm) and micropores (1–30 μm). Micropores were located in between the sintered Ti64 particles on the cell walls and edges, while macrospores formed

Table 1
Chemical composition of Ti64 (wt%) powder (manufacturer's data sheet).

| | Element | | | | | | | | | |
|---|---|---|---|---|---|---|---|---|---|---|
| | Al | V | O | Fe | C | H | N | Cu | Sn | Ti |
| ASTM F1580-1 | 5.5–6.75 | 3.5–4.5 | 0.2 | 0.3 | 0.08 | 0.015 | 0.05 | 0.1 | 0.1 | Bal. |
| Powder | 6.27 | 4.0 | 0.15 | 0.05 | 0.085 | – | 0.011 | – | – | Bal. |

Table 2
Powder sieve analysis (%) (manufacturer's data sheet).

| Opening (μm) | 150 | 105 | 90 | 74 | 63 | 53 | 45 | 30 |
|---|---|---|---|---|---|---|---|---|
| Powder | 99.9 | 68.5 | – | 33.1 | 19.4 | 16.5 | 2.8 | – |

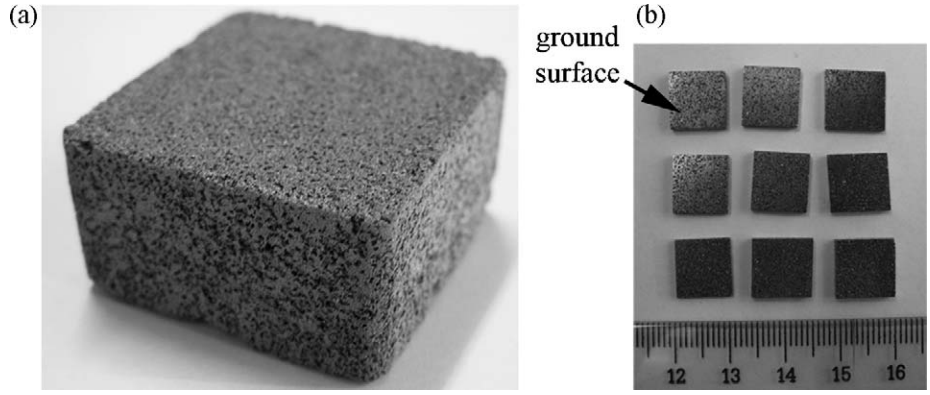


Fig. 1. (a) Foam specimen plate and (b) plate-like foam test specimens for in vitro investigation.

as a result of the space holder removal. The details of the Ti64 foam preparation and the resulting microstructure and mechanical properties are given elsewhere [8].

Small square cross-section plate-like specimens (10 mm × 10 mm × 3 mm) used in vitro investigations were cut from the sintered Ti64 foam plates (Fig. 1(a)), using a low speed diamond saw. The specimens' square cross-sections (Fig. 1(b)) were then ground sequentially using 120, 240, 320, 600, 800, 1200 and 2400 grit SiC papers. The surfaces of foam specimens are therefore composed of ground flat regions and the cells (pores). The foam specimens were then cleaned ultrasonically in acetone, then in ethyl alcohol and finally in deionized water for a duration of 15 min for each solution. Before in vitro tests, Ti64 foam specimens were exposed to three different surface treatments. In acid etching, the foam specimens were immersed into an 1:1:1 volume ratio solution of $H_2SO_4$ (98%), HCl (36%) and $H_2O$ at 60 °C for 1 h. Nitric acid treatment was performed in a 1:1 volume ratio solution of $HNO_3$ (65%) and $H_2O$ at 60 °C for 5 h. In alkali treatment, the specimens were kept in 100 ml 10 M NaOH aqueous solution at 60 °C for 24 h. Following the treatments, the specimens were cleaned ultrasonically in deionized water for 15 min and then AE and nitric acid treated (NAT) specimens were dried in air, while AT specimens were dried in an oven at 40 °C for 24 h.

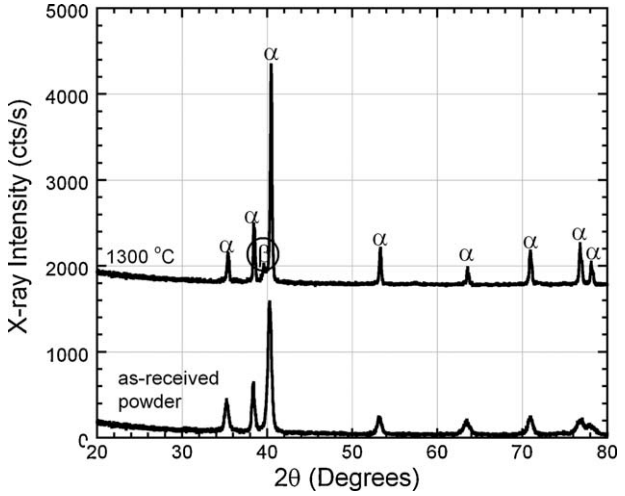


Fig. 2. XRD spectra of as-received Ti64 powder and sintered Ti64 foam.

### 2.2. Bioactivity and characterization

The SBF solution for in vitro tests was prepared by dissolving the following analytical reagents in 1 L of deionized water: 6.547 g of NaCl, 2.268 g of $NaHCO_3$, 0.372 g of KCl, 0.124 g of $NaHPO_4$, 0.305 g of $MgCl_2{\cdot}6H_2O$, 0.368 g of $CaCl_2{\cdot}2H_2O$, 0.071 g of $Na_2SO_4$ and 6.057 g of trishydoxymethylaminomethane. Each foam specimen was placed into a polypropylene tube contained 6 ml SBF solution. The tubes were then kept at 37 °C for 14-day in an incubator. The SBF solution of the tubes was refreshed every 24 h.

The phase identification of the treated and untreated foam specimens before and after in vitro tests was performed using a

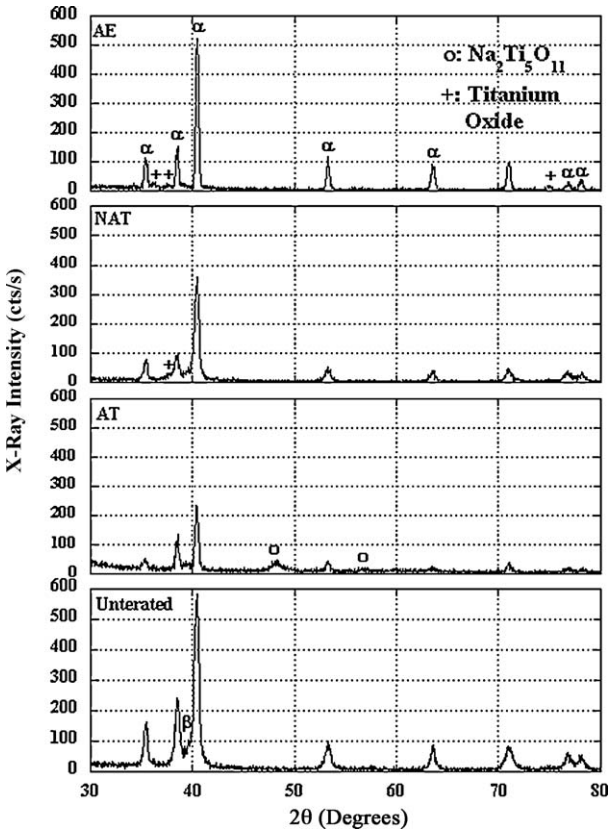


Fig. 3. GIXRD spectra of untreated, AT, NAT and AE specimens before SBF immersion.

Philips Xpert X-ray diffractometer with Cu Kα X-ray (λ = 1.5404 for 8.05 keV). A Philips XL30-SFEG scanning electron microscope (SEM) with an Energy Dispersive X-ray (EDX) analyzer was used for microscopic investigations. A PerkinElmer Attenuated Total Reflectance Fourier Transform Infrared (ATR-FTIR) Spectrometer was used to analyze the band structure of the coating layer. The surface morphology and roughness (*Ra*) of foam specimens before and after in vitro tests were determined using a Nanoscope-IV Atomic Force Microscope (AFM) and taping tips (Otespa, Veecco) with the spring constant of 12–200 N $m^{-1}$. At least three AFM surface scans were performed on the arbitrarily chosen areas of foam specimen's flat ground surfaces. The surface roughness values were calculated by averaging the measured surface roughness values of three scans.

## 3. Results

The XRD spectra of as-received Ti64 powder and sintered Ti64 foam specimen are shown together in Fig. 2. The β phase peak seen in the XRD spectrum of sintered foam specimen (circled in Fig. 2) confirms the microscopically observed transformation of the powder microstructure (not shown here), after sintering at 1300 °C, from fully needle-like α-phase into Widmanstätten microstructure which comprises the colonies of β lathes (bcc and rich in V) and α platelets (hcp and rich in Al). The grazing incidence X-ray diffraction (GIXRD) (incident angle of $\omega = 0.5^{\circ}$) spectra of untreated, AT, NAT and AE foam specimen before SBF immersion are shown in Fig. 3. Titanium oxide peaks seen in the GIXRD spectra of AE and NAT specimen, marked as ''+'', indicate the presence of a relatively thin oxide layer on the foam specimen surfaces. On the other hand, the peaks marked as ''o'' in the spectrum of AT foam specimen in Fig. 3 indicate the formation of a thin $Na_2Ti_5O_{11}$ layer (measured as 500 nm thick from the SEM pictures of the cross-section of AT foam sample particles) on the foam specimen flat surfaces and also on the surfaces of particles in the cells. The untreated foam specimen flat surface before SBF immersion, as is expected, is relatively smooth and shows only few grinding lines (Fig. 4(a) and (c)). Alkali treatment; however, results in a relatively rough surface (Fig. 5(a) and (c)). The surface is mainly composed of a porous $Na_2Ti_5O_{11}$ layer and on this porous layer the cracks are clearly seen (Fig. 5(c)). The crack formation may partly be attributed to the difference

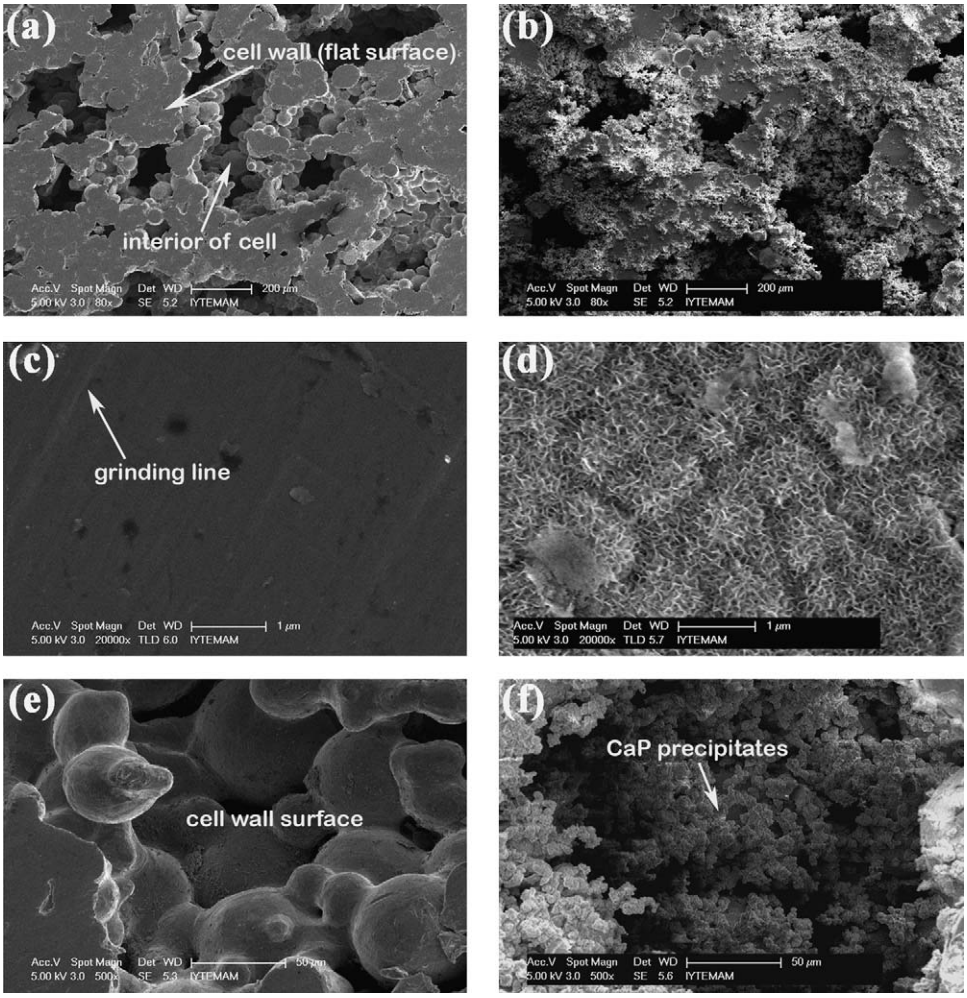


Fig. 4. SEM micrographs of untreated foam specimen flat surface, (a) before and (b) after 14-day of SBF immersion, magnified view of the flat surface, (c) before and (d) after 14-day of SBF immersion and interior of cells, (e) before and (f) after 14-day of SBF immersion.

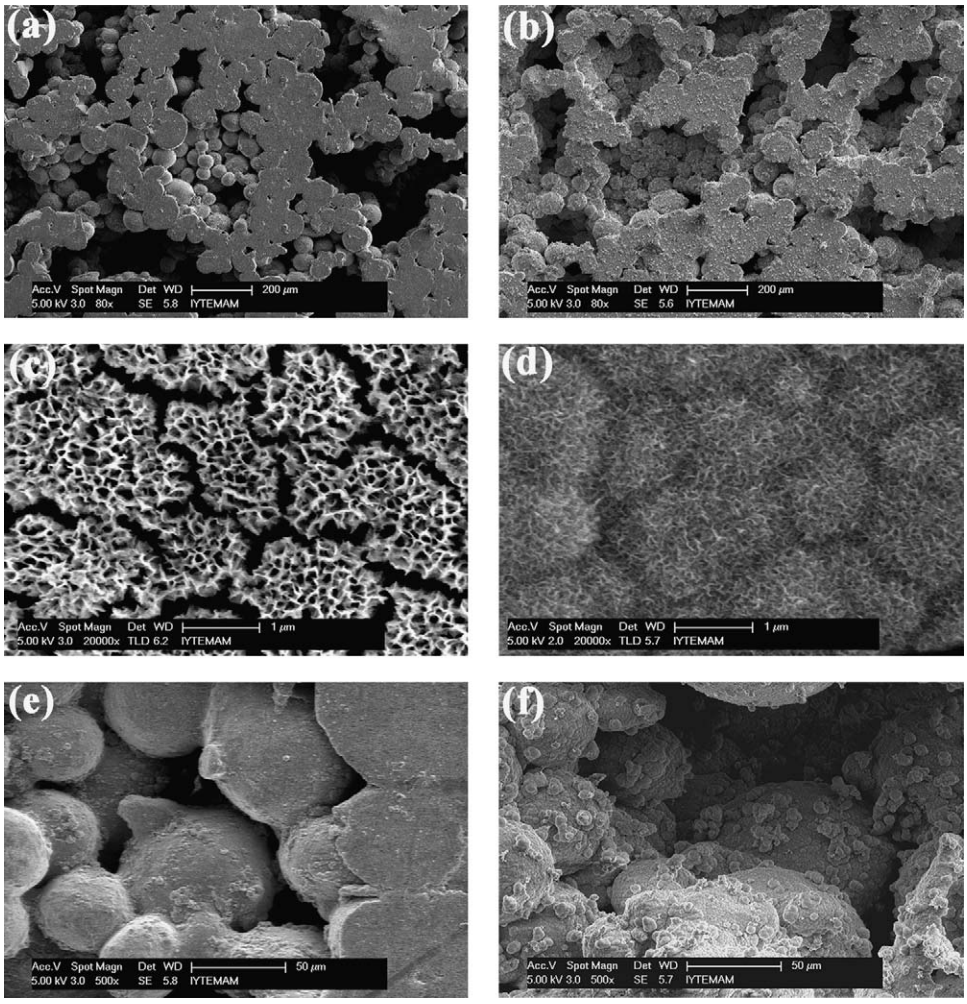


Fig. 5. SEM micrographs of AT foam specimen flat surface, (a) before and (b) after 14-day of SBF immersion, magnified view of the flat surface, (c) before and (d) after 14-day of SBF immersion and interior of cells, (e) before and (f) after 14-day of SBF immersion.

in the thermal expansion coefficient between Ti64 alloy and the surface layer phase ($Na_2Ti_5O_{11}$). On the contrary, nitric acid treatment induces a relatively smooth surface layer which is mainly resulted from the surface oxidation of Ti64 particles, although few large shallow pits and grinding lines are detected on the surface (Fig. 6(a) and (c)). Acid etching is expected to dissolve/remove the natural oxide layer on Ti64 particle surface, presumably being thickened during compact sintering at high temperature. Acid etching is found to result in preferential etching of β lathes of Widmanstätten microstructure as depicted in Fig. 7(a), (c) and (e), proving a higher rate of β phase dissolution in acid etching. Because of this, β phase peaks are not seen and the intensity of the diffraction peaks of α phase increases in the GIXRD spectrum of AE foam specimen in Fig. 3. The acid etching marks seen in Fig. 7(c) and (e) are furthermore noted to be deeper than X-ray penetration depth (∼174 nm). Figs. 4(b), 5(b), 6(b) and 7(b) show sequentially the SEM micrographs of untreated, AT, NAT and AE foam specimen after SBF immersion. The apatite coating layer on untreated foam specimen is considered non-uniform as relatively large size CaP globules are seen on the surface (Fig. 4(b)). In some regions on the surface, the coating layer was further observed to be detached, showing a weak mechanical griping between the foam surfaces and coating layer. Fig. 4(b) also shows that the pores in untreated foam specimens are partially filled with CaP after 14-day of immersion, while the pores are seen to be relatively open in surface treated foam specimens, Figs. 5(b), 6(b) and 7(b).

The coating layer homogeneity in porous structures can only be provided by forming a homogenous coating layer both on the flat surfaces and on the cell wall surfaces. Figs. 4(d) and (e), 5(d) and (e), 6(d) and (e) and 7(d) and (e) show sequentially the SEM micrographs of the cell wall surfaces (inside the pores) of untreated, AT, NAT and AE foam spectrum before and after 14-day of SBF immersion, respectively. After 14-day of SBF immersion the pores between the particles of untreated foam specimens are filled with the globules of CaP precipitates (Fig. 4(e)) and the micropores between sintered Ti64 particles on the cell wall surfaces are further presumably filled with precipitates. In contrast, a continuous CaP coating layer is seen on the cell wall surfaces of AT foam specimen, depicted in Fig. 5(e). It is also noted in the same figure that the micropores remain open after 14-day of SBF immersion. In NAT foam specimen, the CaP layer is found to be relatively thinner and

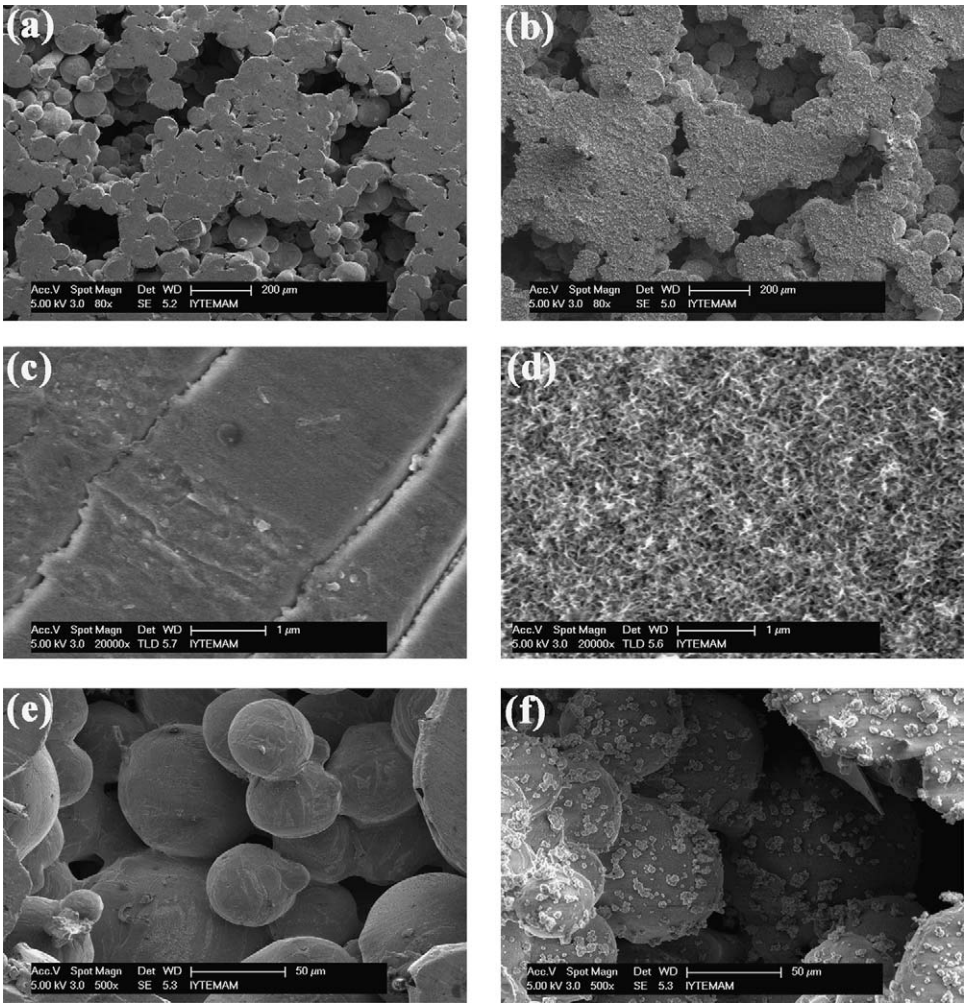


Fig. 6. SEM micrographs of NAT foam specimen flat surface, (a) before and (b) after 14-day of SBF immersion, magnified view of the flat surface, (c) before and (d) after 14-day of SBF immersion and interior of cells, (e) before and (f) after 14-day of SBF immersion.

continuous after 14-day of SBF immersion and tiny separated CaP globules are seen on the particle surface as shown in Fig. 6(e). Lastly, the coating layer on the cell wall surfaces of AE foam specimen is not continuous after 14-day of SBF immersion (Fig. 7(d)).

The GIXRD spectra of untreated AT, NAT and AE foam specimens after 14-day of SBF immersion are shown in Fig. 8(a). The GIXRD spectrum of untreated SBF-immersed specimen shown in this figure is fitted with Gaussian Lorentzion distribution ($R^2 = 0.9$). The fitted spectrum reveals a broad peak at 32°, which is the reflections from (2 1 1), (2 1 2) and (3 0 0) planes of carbonated-hydroxyl apatite (CHA) at 31.037°, 32.057° and 32.998°, respectively. The lattice parameters of hexagonal structure of CHA (JCPDS 9-432) closely match to the calculated lattice parameters of the coating layer ($a = 0.944$ nm and $c = 0.688$ nm). Fig. 8(b) shows the ATR-FTIR analyses of coating layer of the foam specimens after 14-day of SBF immersion. The absorption band at 3450 $cm^{-1}$ and bending mode at 1650 $cm^{-1}$ in Fig. 8(b) are associated with water. The peaks observed at 1040, 604 and 567 $cm^{-1}$ are due to the stretching of $PO_4^{3-}$ vibrations. The peaks seen at 959 and 875 $cm^{-1}$ indicate the presence $HPO_4^{2-}$ group. The bands detected at 1460, 1420 and 875 $cm^{-1}$ further show the presence of $CO_3^{2-}$ group.

The particle flat section surface AFM micrographs (1.5 μm × 1.5 μm) of untreated, AT and NAT foam specimen before and after SBF immersion are shown sequentially in Figs. 9(a) and (b), 10(a) and (b) and 11(a) and (b). The AFM measured *Ra* and *Rq* (root mean square) values before and after SBF immersion are tabulated in Tables 3 and 4 together with the surface area difference (SAD) values, respectively. Since the surface roughness measurements were conducted in a relatively small area, the grinding scratches naturally inducing a macroscale roughness on the surface are avoided in the surface roughness measurements. However, the surface roughness of AE specimens could not be measured in AFM, since the macroscale roughness in these specimens in certain locations was higher than 5 μm, which was a limiting roughness for AFM measurement. As tabulated in Table 3, AT foam specimen shows the highest average surface roughness value (12.642 nm) before SBF immersion. The average surface roughness value of NAT specimen (8.778 nm) is very much similar to that of untreated specimen (8.823 nm). The AFM surface roughness values of foam specimens after SBF immersion (Table 4) are

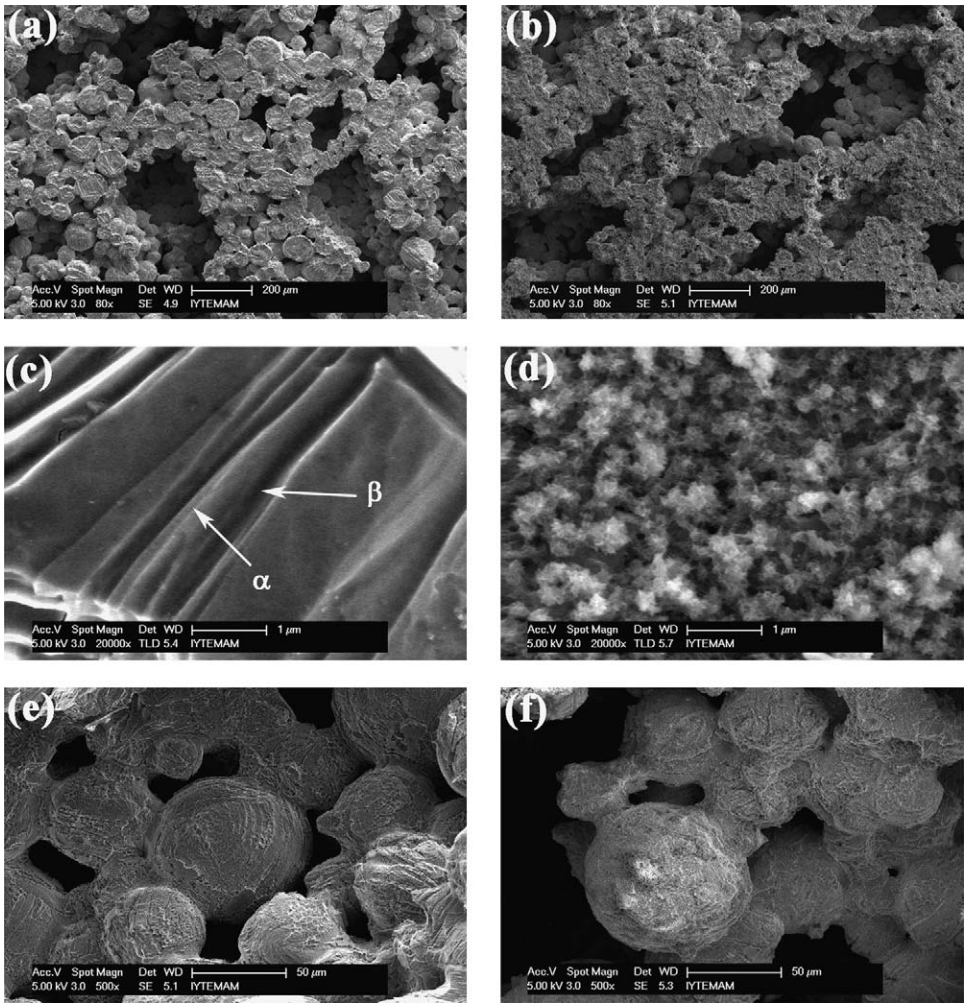


Fig. 7. SEM micrographs of AE foam specimen flat surface, (a) before and (b) after 14-day of SBF immersion, magnified view of the flat surface, (c) before and (d) after 14-day of SBF immersion and interior of cells, (e) before and (f) after 14-day of SBF immersion.

higher than those of untreated and treated foam specimens before SBF immersion (Table 3). SBF immersion clearly increases surface roughness of untreated and treated foam specimens. After SBF immersion, the surface roughness values increase at least 3.2 times of the surface roughness values before SBF immersion (Tables 3 and 4). It is also noted in Tables 3 and 4 that AT foam specimen has the highest surface roughness value before and after SBF immersion.

## 4. Discussion

In alkali solutions, the surface passive $TiO_2$ layer on Ti partially dissolves by the corrosive attack of hydroxyl group, producing negatively charged hydrates based on the following reaction [21,22]

$$TiO_2{\cdot}nH_2O + OH^- \rightarrow HTiO_3^-{\cdot}nH_2O \quad (1)$$

The negatively charged $HTiO_3^-{\cdot}nH_2O$ reacts with alkali ions in aqueous solution, forming a porous thin sodium titanate layer on the surface of Ti [18,19,22,23]. This porous structure was presumed to result from the local corrosion action of $OH^-$ radicals. The morphology of this layer changes with the surface treatment conditions and also with the applied heat-treatment process [18]. The mechanisms of apatite formation on alkali and heat treated Ti have recently been demonstrated based on the electrostatic interactions between the ions in SBF and Ti surface by Kukoba [23]. It was proposed that initially sodium titanate layer releases $Na^+$ ions by exchanging with $H_3O^+$ ions in the SBF, forming Ti–OH functional groups on the surface. Then, the reaction between the positively charged $Ca^{2+}$ ions in the SBF and negatively charged Ti–OH functional group on the surface results in the formation of a calcium titanate layer. Later, this layer is replaced by an amorphous calcium phosphate layer through the reaction between the positively charged Ti surface resulting from Ca accumulation and the negatively charged phosphate ions in SBF. The calcium phosphate layer finally transforms into a stable crystalline bonelike apatite. The function of the heat-treatment process applied following the alkali treatment was shown to increase the crystallization of the gel layer and to enhance the adhesion of sodium titanate layer to Ti surface, while it had no beneficial effect on the reduction of the induction period of the apatite

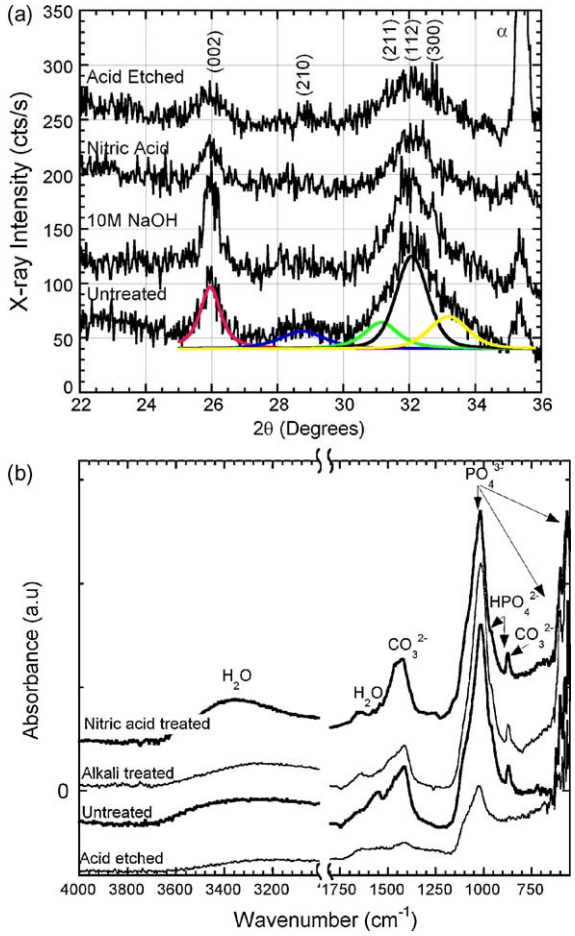


Fig. 8. (a) GIXRD spectra of untreated, AT, NAT and AE foam specimen after 14-day of SBF immersion and (b) ATR-FTIR analyses of foam specimens after 14-day of SBF immersion.

formation in SBF [21]. The applied subsequent heat-treatment process was previously shown to result in oxide formation on the surface [21], which may increase the total oxygen content of Ti64 particles. The effect of heat-treatment process on CaP precipitation of studied foams will be investigated in future in a separate study.

Acid ($HCl + H_2SO_4$) etching was shown to dissolve the natural oxide layer and form a relatively rough surface on Ti [24]. In contrast, nitric acid treatment was found not to affect the surface roughness, but increased the surface energy [25]. In the present study, the AFM surface roughness of NAT specimens is found to be nearly the same with that of the untreated specimen, agreeing with the results of Lu et al. [25] and Sittig et al. [26]. This further proves the non-preferential etching and low dissolution rates of α and β phase in nitric acid. Barrere et al. [27] showed that the surface topography of Ti64 had no affect on the heterogeneous nucleation of CaP, while the growth and mechanical attachment of CaP coating strongly depended on the surface roughness; a rougher surface ($R_{max} > 0.1$ μm) was much more effective for the CaP mechanical attachment to the surface.

Alkali treatment induces a smaller crystal size on the surface than nitric acid treatment and acid etching, which is reflected by the increased intensity of (0 0 2) diffraction line of AT specimen shown in Fig. 8(a). The reduced crystal size of the CaP layer of AT foam specimen is also seen in the AFM micrographs of Fig. 10(a) and (b). This is partly attributed to the increased number of heterogeneous nucleation sites in AT foam specimen surfaces.

Fig. 12(a–d) shows sequentially the magnified SEM micrographs of untreated, AT, NAT and AE foam specimen particle(s) interior of the cells. Although in untreated foam specimen, the particles interior of the cells are coated with CaP

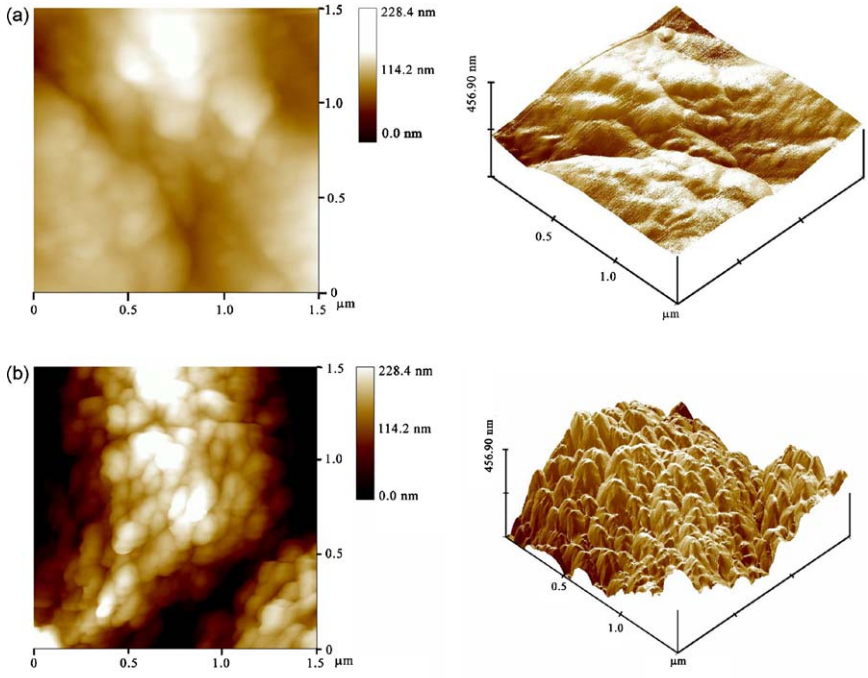


Fig. 9. 2D and 3D AFM micrographs of surface topologies of untreated foam specimen (a) before and (b) after 14-day of SBF immersion.

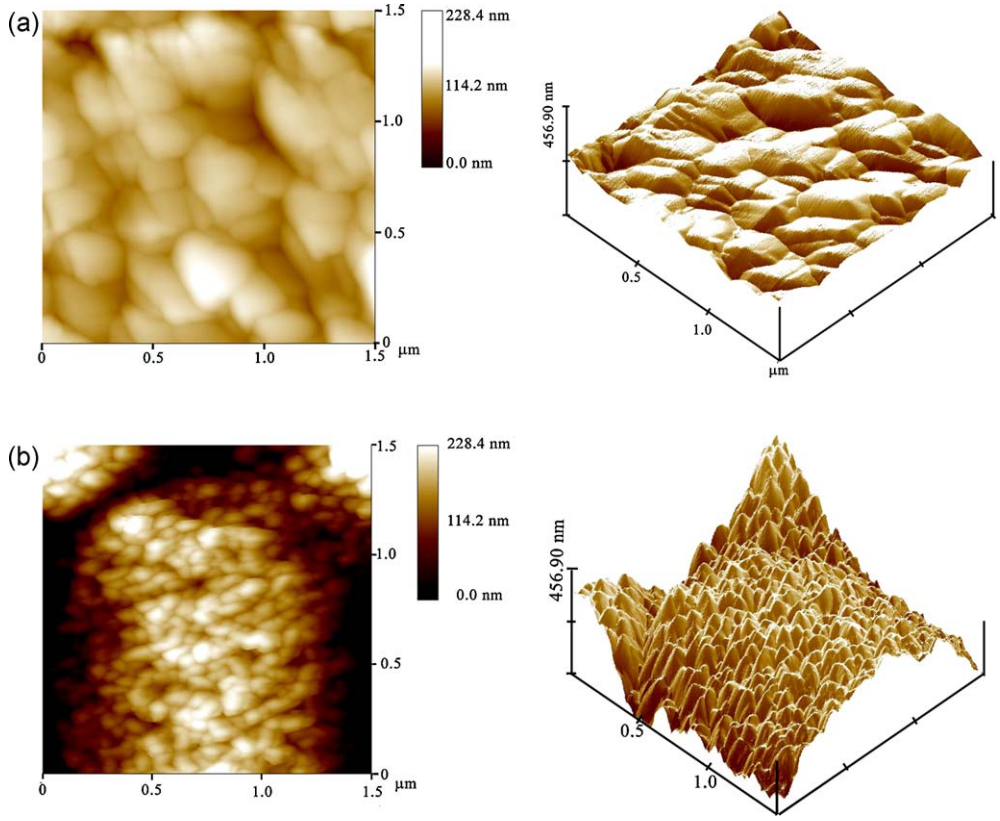


Fig. 10. 2D and 3D AFM micrographs of surface topologies of AT foam specimen (a) before and (b) after 14-day of SBF immersion.

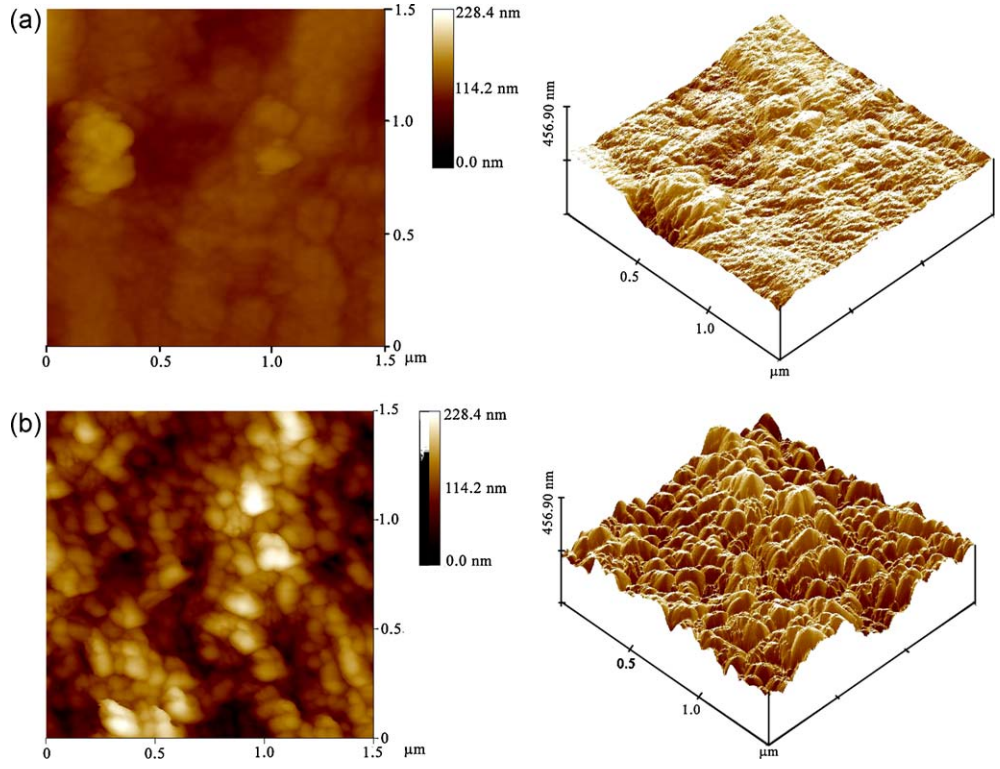


Fig. 11. 2D and 3D AFM micrographs of surface topologies of NAT foam specimen (a) before and (b) after 14-day of SBF immersion.

Table 3
Surface roughness of foam flat surfaces before SBF immersion.

| | *Ra* (nm) | *Rq* (nm) | SAD (%) |
|---|---|---|---|
| As-received | 8.823 | 10.715 | 1.279 |
| NA | 8.778 | 12.012 | 3.832 |
| AT | 12.642 | 15.769 | 5.477 |

Table 4
Surface roughness of foam flat surfaces after 14-day of SBF immersion.

| | *Ra* (nm) | *Rq* (nm) | SAD (%) |
|---|---|---|---|
| HA + as-received | 32.035 | 41.236 | 16.659 |
| NA + HA | 28.394 | 35.442 | 41.581 |
| AT + HA | 60.15 | 72.748 | 59.286 |

layer, as stated previously, the interior of the cells and the micropores between particles are filled with precipitates as seen in Fig. 12(a). Alkali treatment however results in homogenous CaP deposition on the cell wall surfaces and the micropores remain open after SBF immersion. Few CaP precipitate globules and relatively large cracks are seen on this continuous coating layer as shown in Fig. 12(b). Fig. 13 shows the SEM micrograph of the cross-section of a CaP coated Ti64 particle in

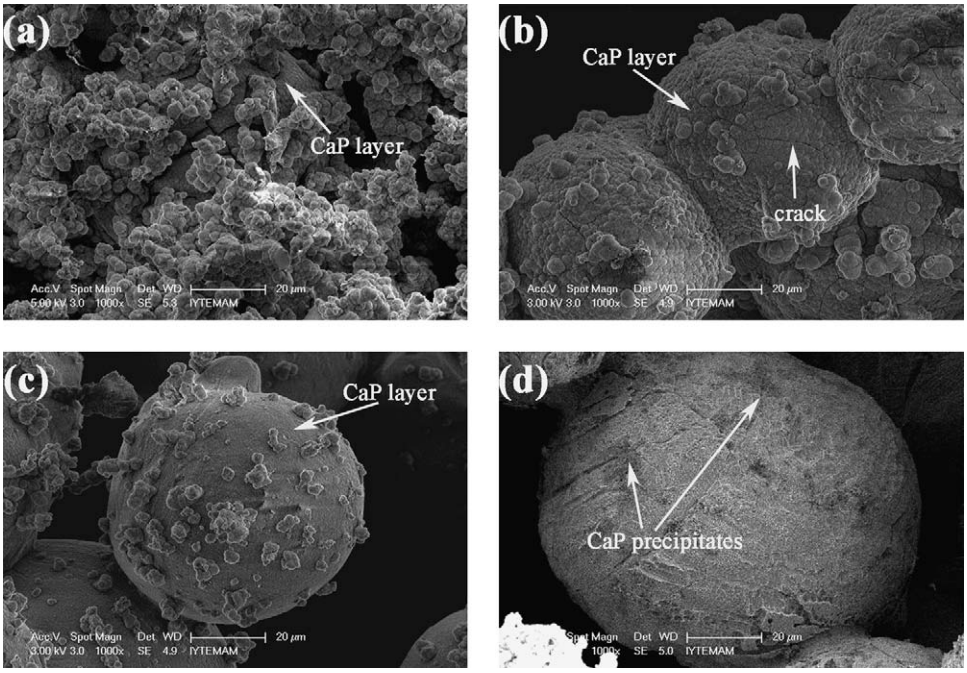


Fig. 12. CaP deposition on the particles at cell wall surfaces (inside the cells); (a) untreated, (b) AT, (c) NAT and (d) AE specimens after 14-day of SBF immersion.

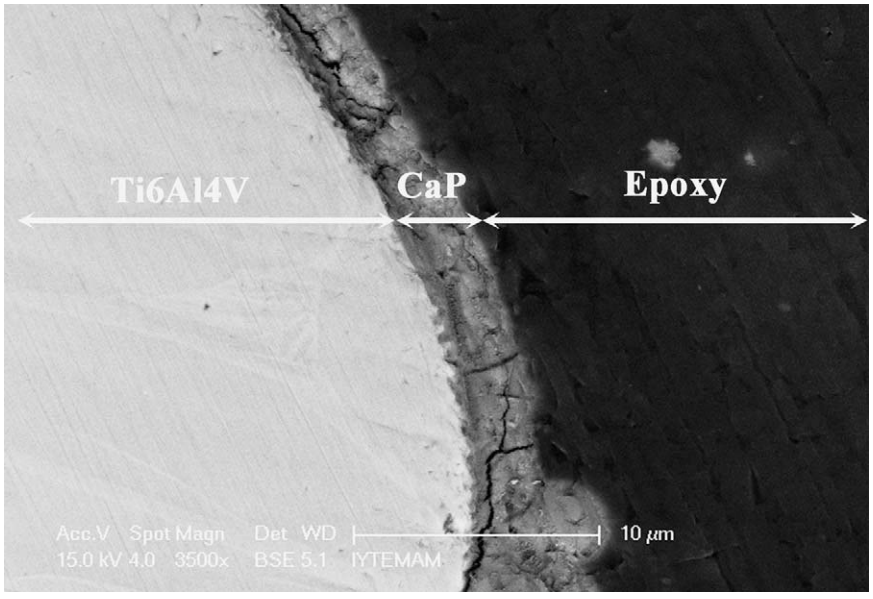


Fig. 13. SEM micrograph showing the cross-section of CaP coating on a Ti64 particle.

an AT foam specimen. The coating layer has nearly uniform thickness, ∼3 μm, and accommodates lateral cracks on the cross-section (Fig. 13). A similar observation was previously reported by Zhang et al. [15] in the SBF immersion of an open cell Ti foam. In NAT foam specimens, CaP precipitate globules are seen on the particles interior of the cells (Fig. 12(c)). Underneath the CaP globules, a homogeneous and relatively thinner CaP coating layer is seen (Fig. 12(c)). The thickness of CaP layer could however not be determined through the polished particles cross-sections as the coating layer probably broke during the specimen preparation. The thickness of CaP layer in these specimens was measured as 0.6 μm from the SEM micrographs of the coating layer accommodating cracked sections. Since the coating layer thickness is thinner, the extend of coating cracks is greatly reduced in NAT foam specimens as compared with AT foam specimens. In AE foam specimens, only CaP precipitates are found on the surfaces of the particles interior of the cells (Fig. 12(d)).

The results of the present study have clearly shown that nitric acid treatment can be used, in addition to widely used alkali treatment, in the biomimetic coating of Ti64 open cell foams. However, the effect of the surface treatment type on the adhesion of CaP coating should be evaluated for the same thicknesses of coating layer before selecting the type of surface treatment applicable to Ti64 open cell foams.

## 5. Conclusions

In the present study, the effects of commonly used surface treatments, including alkali and nitric acid treatment and acid etching, on the CaP deposition of an open cell Ti64 foam (60% porous and 300–500 μm pro size) were investigated in a SBF solution for 14-day. Untreated foam specimens were also tested for comparison. The surface roughnesses of the foam specimens flat surfaces were measured in nano-metric scale before and after SBF immersion using AFM. Although nitric acid treatment was found not to affect the surface roughness, alkali treatment increased the surface roughness as compared with untreated foam specimen in nano-metric scale. The surface roughness of the foam specimens further increased with CaP deposition in SBF. A significant increase in the surface roughness of alkali treated foam specimens as compared with untreated and nitric acid treated specimens following the SBF immersion further proved the smaller crystal size CaP deposition. This result was also confirmed by the AFM micrographs taken from the foam specimens surfaces after SBF immersion. Although, acid etching preferentially dissolved β-phase, nitric acid treatment showed relatively low and equal dissolution rates of α- and β-phase of the Widmanstätten structure of the studied Ti64 foams. The AFM measured nano-scale surface roughness of nitric acid treated foam specimens also agreed with this result. The microscopic evaluation of the CaP deposition on the cell wall surfaces of foam (interior of cells) clearly showed that alkali treatment and nitric acid treatment induced a continuous uniform CaP layer deposition. The coating thickness was measured as ∼3 and ∼0.6 μm in AT and NAT specimen after 14-day of SBF immersion.

## References


[1] R.M. Pilliar, Porous-surfaced metallic implants for orthopedic applications, Journal of Biomedical Materials Research-Applied Biomaterials 21 (A1) (1987) 1–33.

[2] M. Long, H.J. Rack, Titanium alloys in total joint replacement – a materials science perspective, Biomaterials 19 (18) (1998) 1621–1639.

[3] G. Ryan, A. Pandit, D.P. Apatsidis, Fabrication methods of porous metals for use in orthopaedic applications, Biomaterials 27 (13) (2006) 2651–2670.

[4] I.H. Oh, N. Nomura, N. Masahashi, S. Hanada, Mechanical properties of porous titanium compacts prepared by powder sintering, Scripta Materialia 49 (12) (2003) 1197–1202.

[5] M. Guden, E. Celik, A. Hizal, M. Altindis, S. Cetiner, Effects of compaction pressure and particle shape on the porosity and compression mechanical properties of sintered Ti6Al4V powder compacts for hard tissue implantation, Journal of Biomedical Materials Research Part B-Applied Biomaterials 85B (2) (2008) 547–555.

[6] M. Guden, E. Celik, E. Akar, S. Cetiner, Compression testing of a sintered Ti6Al4V powder compact for biomedical applications, Materials Characterization 54 (4–5) (2005) 399–408.

[7] C.E. Wen, M. Mabuchi, Y. Yamada, K. Shimojima, Y. Chino, T. Asahina, Processing of biocompatible porous Ti and Mg, Scripta Materialia 45 (10) (2001) 1147–1153.

[8] M.E. Dizlek, M. Guden, U. Turkan, A. Tasdemirci, Processing and compression testing of Ti6Al4V foams for biomedical applications, Journal of Materials Science 44 (6) (2009) 1512–1519.

[9] T. Tsukeoka, M. Suzuki, C. Ohtsuki, Y. Tsuneizumi, J. Miyagi, A. Sugino, T. Inoue, R. Michihiro, H. Moriya, Enhanced fixation of implants by bone ingrowth to titanium fiber mesh: effect of incorporation of hydroxyapatite powder, Journal of Biomedical Materials Research Part B-Applied Biomaterials 75B (1) (2005) 168–176.

[10] J.W.M. Vehof, P.H.M. Spauwen, J.A. Jansen, Bone formation in calcium-phosphate-coated titanium mesh, Biomaterials 21 (19) (2000) 2003–2009.

[11] H.Q. Nguyen, D.A. Deporter, R.M. Pilliar, N. Valiquette, R. Yakubovich, The effect of sol–gel-formed calcium phosphate coatings on bone ingrowth and osteoconductivity of porous-surfaced Ti alloy implants, Biomaterials 25 (5) (2004) 865–876.

[12] A. Tache, L. Gan, D. Deporter, R.M. Pillar, Effect of surface chemistry on the rate of osseointegration of sintered porous-surfaced Ti–6Al–4V implants, International Journal of Oral & Maxillofacial Implants 19 (1) (2004) 19–29.

[13] F.J. Gil, A. Padros, J.M. Manero, C. Aparicio, M. Nilsson, J.A. Planell, Growth of bioactive surfaces on titanium and its alloys for orthopaedic and dental implants, Materials Science & Engineering C-Biomimetic and Supramolecular Systems 22 (1) (2002) 53–60.

[14] W.Q. Yan, T. Nakamura, K. Kawanabe, S. Nishigochi, M. Oka, T. Kokubo, Apatite layer-coated titanium for use as bone bonding implants, Biomaterials 18 (17) (1997) 1185–1190.

[15] Q.Y. Zhang, Y. Leng, R.L. Xin, A comparative study of electrochemical deposition and biomimetic deposition of calcium phosphate on porous titanium, Biomaterials 26 (16) (2005) 2857–2865.

[16] F.H. Liang, L. Zhou, K.G. Wang, Apatite formation on porous titanium by alkali and heat-treatment, Surface & Coatings Technology 165 (2) (2003) 133–139.

[17] D.D. Deligianni, N.D. Katsala, P.G. Koutsoukos, Y.F. Missirlis, Effect of surface roughness of hydroxyapatite on human bone marrow cell adhesion, proliferation, differentiation and detachment strength, Biomaterials 22 (1) (2001) 87–96.

[18] M Wei, H.M. Kim, T. Kokubo, J.H. Evans, Optimising the bioactivity of alkaline-treated titanium alloy, Materials Science & Engineering C-Biomimetic and Supramolecular Systems 20 (1–2) (2002) 125–134.

[19] B.H. Lee, Y.D. Kim, J.H. Shin, K.H. Lee, Surface modification by alkali and heat treatments in titanium alloys, Journal of Biomedical Materials Research 61 (3) (2002) 466–473.

[20] ASTM F 1580-95, Standard specification for titanium and Ti6Al4V alloy powders for coating surgical implants.

[21] H.M. Kim, F. Miyaji, T. Kokubo, T. Nakamura, Effect of heat treatment on apatite-forming ability of Ti metal induced by alkali treatment, Journal of Materials Science-Materials in Medicine 8 (6) (1997) 341–347.
[22] H.M. Kim, F. Miyaji, T. Kokubo, T. Nakamura, Preparation of bioactive Ti and its alloys via simple chemical surface treatment, Journal of Biomedical Materials Research 32 (3) (1996) 409–417.
[23] T. Kokubo, Development of bioactive materials based on surface chemistry, Journal of the European Ceramic Society 29 (7) (2008) 1267–1274.
[24] X. Lu, Y.B. Wang, X.D. Yang, Q.Y. Zhang, Z.F. Zhao, L.T. Weng, Y. Leng, Spectroscopic analysis of titanium surface functional groups under various surface modification and their behaviors in vitro and in vivo, Journal of Biomedical Materials Research Part A 84A (2) (2008) 523–534.
[25] X. Lu, Z.F. Zhao, Y. Leng, Biomimetic calcium phosphate coatings on nitric-acid-treated titanium surfaces, Materials Science & Engineering C-Biomimetic and Supramolecular Systems 27 (4) (2007) 700–708.
[26] C. Sittig, M. Textor, N.D. Spencer, M. Wieland, P.H. Vallotton, Surface characterization of implant materials cp Ti, Ti–6Al–7Nb and Ti–6Al–4V with different pretreatments, Journal of Materials Science-Materials in Medicine 10 (1) (1999) 35–46.
[27] F. Barrere, M.M.E. Snel, C.A. van Blitterswijk, K. de Groot, P. Layrolle, Nano-scale study of the nucleation and growth of calcium phosphate coating on titanium implants, Biomaterials 25 (14) (2004) 2901–2910.